

## Supporting Information

### Single crystalline zinc stannate nanoparticles for efficient photo-electrochemical devices

Masahiro Miyauchi\*, Zhifu Liu, Zhi-Gang Zhao, Srinivasan Anandan, Kohjiro Hara\*  
*National Institute of Advanced Industrial Science and Technology (AIST), Tsukuba Central 5,  
1-1-1 Higashi, Tsukuba, Ibaraki 305-8565, Japan*

E-mail: [m-miyauchi@aist.go.jp](mailto:m-miyauchi@aist.go.jp), [k-hara@aist.go.jp](mailto:k-hara@aist.go.jp)

### Experimental

#### Hydrothermal Synthesis

Both  $\text{ZnSnO}_3$  and  $\text{Zn}_2\text{SnO}_4$  were prepared by a hydrothermal reaction. Zinc acetate dihydrate ( $\text{Zn}(\text{CH}_3\text{COO})_2 \cdot 2\text{H}_2\text{O}$ ) and tin tetrachloride pentahydrate ( $\text{SnCl}_4 \cdot 5\text{H}_2\text{O}$ ) were used as raw materials. The raw materials were dissolved in an aqueous sodium hydroxide (NaOH) solution with a total metal ion concentration of 0.25 mol/L. Each solution had a volume of 50 mL, and was stirred at room temperature for 30 min. Then the solutions were placed into a 100 mL Teflon-lined autoclave, and hydrothermally reacted in an oven. As shown in Table S1, we changed various synthesis conditions, including the Zn:Sn ratio, concentration of NaOH, and reaction temperature. After hydrothermal reactions, the autoclave was cooled to room temperature, and precipitates were filtered and washed with pure water. The corrected products were dried at 60 °C to obtain powder forms.

Table S1. Synthesis conditions and crystal phases of products

sample	Zn/Sn	NaOH (M)	Temperature (K)	Products
1	1 / 1	1	453	$\text{SnO}_2$
2	1 / 1	1.5	453	$\text{SnO}_2$ , ZnO
3	1 / 1	2	453	$\text{SnO}_2$ , ZnO, $\text{ZnSnO}_3$
4	1 / 1	3	453	ZnO, $\text{ZnSnO}_3$
5	1 / 1	7	453	ZnO, $\text{ZnSnO}_3$
6	1 / 1	10	453	$\text{ZnSnO}_3$
7	2 / 1	3	453	$\text{SnO}_2$ , ZnO
8	1 / 2	3	453	ZnO, $\text{SnO}_2$ , $\text{Zn}_2\text{SnO}_4$
9	1 / 4	3	453	$\text{Zn}_2\text{SnO}_4$
10	1 / 1	10	423	$\text{ZnSnO}_3$
11	1 / 4	3	423	ZnO, $\text{Zn}_2\text{SnO}_4$

### ***Characterization and Evaluations***

A scanning electron microscope (SEM, S-4800, Hitachi Ltd.) and a transmission electron microscope (TEM, H-1500, Hitachi, Ltd.) were used to observe the microstructures of the powders and thin films, whereas the crystal phases were evaluated by X-ray diffraction with Cu K $\alpha$  X-rays (XRD model Ultima-X, Rigaku Ltd.). Chemical and thermal stabilities of the powders were investigated by XRD and SEM analyses. Powder samples were immersed in 0.2 M HNO<sub>3</sub> aqueous solution for the acidic treatment, and they were immersed in 0.2 M NaOH aqueous solution for alkali treatment. We measured the XRD and SEM for powder samples before and after treating with acid or alkali. To investigate the thermal stability, XRD and SEM for ZnSnO<sub>3</sub> and Zn<sub>2</sub>SnO<sub>4</sub> powder were recorded after annealing in air at 673 K. The UV-vis diffuse reflectance spectra for the powders were recorded on a spectrophotometer (V-660, JASCO Ltd.), and the absorption coefficients ( $\alpha$ ) for the powders were determined by the Kubelka–Munk method.<sup>1</sup> The nitrogen adsorption isotherms for the powders were evaluated by an adsorption apparatus (Belsorp-2, Bel Japan Ltd.) to measure BET surface area.

The photocatalytic oxidation activities of the powders were evaluated by gaseous acetaldehyde decomposition. The concentrations of acetaldehyde and generated carbon dioxide (CO<sub>2</sub>) were measured by a photoacoustic multigas monitor (model 1312, Innova, Ballerup, Denmark), which had a detection limit of approximately 0.1 ppm. A total of 0.1 g of powder was placed onto a circular glass dish (7.1 cm<sup>2</sup>), which was then set in a 0.5 dm<sup>3</sup> glass vessel. An O<sub>2</sub> (20%)-N<sub>2</sub> (80%) gaseous mixture, which was passed through a 20 °C water humidifier to adjust the relative humidity to 40%, filled the vessel. The headspace (100 cm<sup>3</sup>) of the glass bottle reservoir, which contained liquid acetaldehyde, was injected into the glass vessel using a syringe. The initial concentration of acetaldehyde was 500 ppm. The photocatalytic decomposition of gaseous acetaldehyde was evaluated under UV light irradiation provided by a

Hg-Xe lamp (Luminar Ace 210, Hayashi Watch Works Co., Tokyo, Japan). UV light was irradiated onto the powder samples through glass filters (UVD-36B, Asahi Techno Glass Ltd.) to cutoff short wavelengths below 320 nm because UV light with short wavelengths could react with oxygen molecules to produce ozone. Under our light irradiating condition, acetaldehyde could not decompose without a catalyst. The UV light intensity was  $40 \text{ mW/cm}^2$ , measured by a spectroradiometer (USR-40D, Ushio Ltd.). The present photocatalysis evaluation was monitored under light-limited condition in which the reaction rate strongly depended on the electron-hole charge separation efficiency.<sup>2</sup>

To measure dye-sensitized solar cell performance, thin-film electrodes based on zinc stannate particles were prepared by a screen-printing technique. The organic pastes for screen-printing were composed of  $\text{Zn}_2\text{SnO}_4$  powder, ethyl cellulose as a binder, and  $\alpha$ -terpineol as a solvent. The paste was printed on a glass substrate coated with transparent conducting oxide (TCO, F-doped  $\text{SnO}_2$ , Asahi Glass Co.) and subsequently sintered at  $500 \text{ }^\circ\text{C}$  in air for 1 hour. The thicknesses of the thin films, measured with an Alpha-Step 300 profiler (Tencor Instruments), were ca.  $6 \text{ }\mu\text{m}$ . The sensitizer was an organic dye (MK-2).<sup>3,4</sup> The dye molecules were dissolved in toluene at a concentration of  $0.3 \text{ mM}$ . The electrodes were immersed in the dye solution, and then kept at  $25 \text{ }^\circ\text{C}$  for at least 12 hours to allow the dye to adsorb onto the surface of the electrodes. The sealed electrochemical cell used for photovoltaic measurements consisted of dye-sensitized zinc stannate working electrodes, a Pt-coated TCO counter electrode, a spacer (surlyn film,  $30 \text{ }\mu\text{m}$  thick), and an electrolyte. The counter electrode consisted of a Pt film (ca.  $200 \text{ nm}$  thick) sputtered onto a TCO-coated glass plate. The electrolyte was  $0.6 \text{ M}$  1,2-dimethyl-3-n-propylimidazolium iodide,  $0.1 \text{ M LiI}$ ,  $0.05 \text{ M I}_2$ ,  $0.5 \text{ M}$  4-*tert*-butylpyridine in acetonitrile. The action spectra of the monochromatic incident photon-to-current conversion efficiency (IPCE) of the DSSC were measured with a CEP-99W system (Bunkoh-keiki).

### Formation of single crystalline zinc stannate

Table S1 shows the crystal phases of the products for various synthesis conditions. The ratio of Zn:Sn and the pH value were important parameters for the crystal formation of zinc stannate. When the ratio of Zn:Sn was 1:1, pure ZnSnO<sub>3</sub> was formed under the high alkaline condition with a NaOH concentration of 10 M. In contrast, ZnO or SnO<sub>2</sub> was formed under the low alkaline condition. The formation of ZnSnO<sub>3</sub> is based on the following reaction:



Before hydrothermal treatment, solutions were translucent and composed of amorphous particles, which are considered to be hydroxide nanoparticles such as Zn(OH)<sub>2</sub> or Sn(OH)<sub>4</sub>. During the hydrothermal condition, these hydroxides gradually dissolved at the interface between the surface of the precursor and solution, then oxide nanocrystals nucleated and grew further into ZnSnO<sub>3</sub> particles. Under this reaction, NaOH acted as a mineralizer, and it could hydrolyze zinc and tin salts. Therefore, a high concentration of NaOH effectively formed a highly pure ZnSnO<sub>3</sub> powder. In contrast, Zn<sub>2</sub>SnO<sub>4</sub> was formed when the NaOH concentration was 3.0 M. Highly pure Zn<sub>2</sub>SnO<sub>4</sub> was formed under a Zn:Sn ratio of 1:4 with a pH value of 3.0 (sample No. 9), while ZnO and SnO<sub>2</sub> were formed under a Zn:Sn ratio of 2:1 with a pH value of 3.0 (sample No. 7). It was surprising that the low Zn:Sn ratio condition effectively formed Zn<sub>2</sub>SnO<sub>4</sub>. These phenomena were due to the different solubilities of the raw materials and free energy to form crystalline metal oxide. Previous studies have reported that zinc oxide easily forms at room temperature,<sup>5-7</sup> indicating that crystal growth of ZnO is easier than that of SnO<sub>2</sub>. Therefore, the low Zn:Sn ratio condition effectively formed Zn<sub>2</sub>SnO<sub>4</sub> in our experimental conditions. We have also confirmed that both ZnSnO<sub>3</sub> and Zn<sub>2</sub>SnO<sub>4</sub> were produced even at the reaction temperature of 423 K (samples No. 10 and 11).

### Thermal stability of zinc stannate nanocrystals

Figure S1 shows the XRD patterns of  $\text{ZnSnO}_3$  and  $\text{Zn}_2\text{SnO}_4$  before and after annealing in air at 673 K. Although annealing did not significantly change the XRD pattern of  $\text{Zn}_2\text{SnO}_4$ , that of  $\text{ZnSnO}_3$  became amorphous after heat treatment at 673 K. This amorphous sample was further altered to  $\text{SnO}_2$  and  $\text{Zn}_2\text{SnO}_4$  mixed phases after annealing at 973 K. Because a heat treatment at 773 K is required to construct an electrode on TCO glass to decompose organic substances in the paste, we could not evaluate the dye-sensitized solar cell property of  $\text{ZnSnO}_3$ .

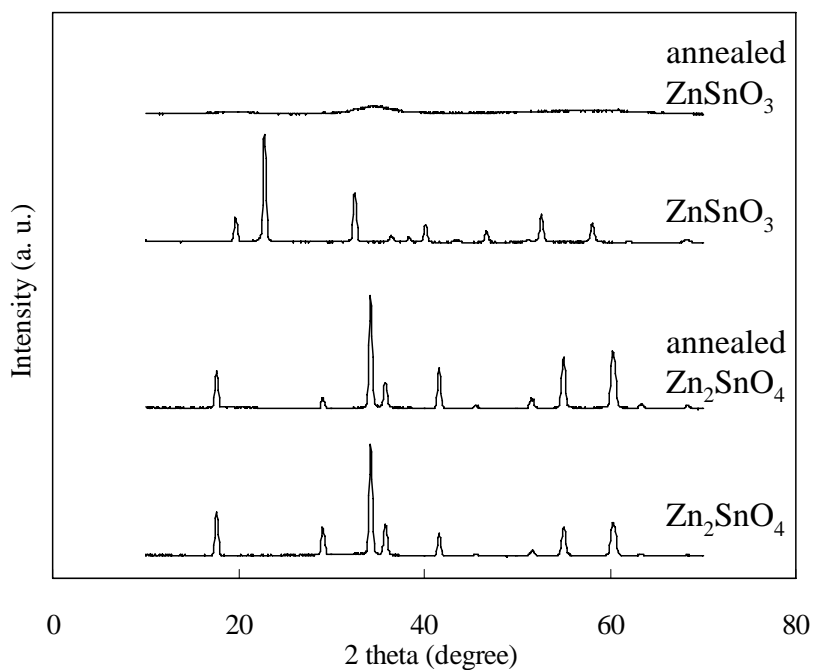


**Figure S1.** XRD patterns for  $\text{Zn}_2\text{SnO}_4$  and  $\text{ZnSnO}_3$  before and after annealing in air at 673 K.

## Photocatalysis

Figure S2 shows the generation of carbon dioxide (CO<sub>2</sub>) by photocatalytic oxidation of acetaldehyde under UV irradiation. This evaluation was monitoring under light-limited conditions where the reaction rate strongly depended on the electron-hole charge separation efficiency.<sup>2</sup> Among these samples, annealed Zn<sub>2</sub>SnO<sub>4</sub> exhibited the highest activity. ZnSnO<sub>3</sub> was less active than Zn<sub>2</sub>SnO<sub>4</sub>. Because the absorption properties differed for these samples, we calculated the reaction rate (*RR*) versus absorbed photon numbers (*PN*). The *PN* value was calculated using the following equation:

$$PN = \int I \cdot \frac{100 - R}{100} d\lambda,$$

where *I* and *R* are the incident photon flux and diffuse reflectance spectra for powder, respectively. The calculated *RR/PN* values for ZnSnO<sub>3</sub>, Zn<sub>2</sub>SnO<sub>4</sub>, and annealed Zn<sub>2</sub>SnO<sub>4</sub> were 1.1×10<sup>-20</sup>, 2.7×10<sup>-20</sup>, 7.7×10<sup>-20</sup> (ppmv/photons), respectively. These results indicate that the quantum yield of Zn<sub>2</sub>SnO<sub>4</sub> without annealing is three times higher than that of ZnSnO<sub>3</sub>. Furthermore, annealing Zn<sub>2</sub>SnO<sub>4</sub> enhances the photocatalytic activity. The differences in the photocatalytic activities of these powders are attributed to their crystallinity. Photocatalysis includes electron-hole carrier separation and reactions with organic substances at a surface. Hence, a higher crystallinity and surface area are key factors for an efficient reaction. The inset shows the complete decomposition of acetaldehyde on annealed Zn<sub>2</sub>SnO<sub>4</sub>. The initial concentration of acetaldehyde was 500 ppm. However, if acetaldehyde was completely mineralized, the concentration of generated carbon dioxide would be 1000 ppm. Therefore, we confirmed that gaseous acetaldehyde molecules almost completely decomposed into carbon dioxide by the photocatalytic oxidation reaction.

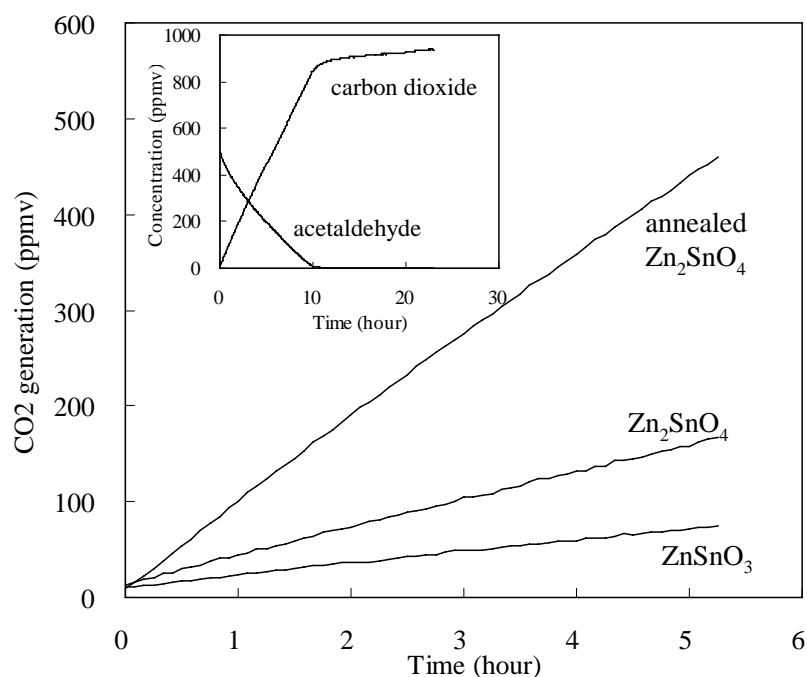


**Figure S2.** Photocatalytic decomposition of gaseous acetaldehyde for zinc stannate nanocrystals under UV irradiation provided by a Hg-Xe lamp (UV intensity: 40 mW/cm<sup>2</sup>). Inset shows the changes in the concentrations of acetaldehyde and CO<sub>2</sub> for annealed Zn<sub>2</sub>SnO<sub>4</sub> (673K).

## References:

- (1) P. Kubelka, F. Munk, *Z. Tech. Phys.*, 1931, 12, 593-601.
- (2) Y. Ohko, K. Hashimoto, A. Fujishima, *J. Phys. Chem. A*, 1997, 101, 8057-8062.
- (3) N. Koumura, Z. S. Wang, S. Mori, M. Miyashita, E. Suzuki, K. Hara, *J. Am. Chem. Soc.*, 2006, 128, 14256–14257 (Addition and correction, 2008, 130, 4202).
- (4) Z.-S. Wang, N. Koumura, Y. Cui, M. Takahashi, H. Sekiguchi, A. Mori, T. Kubo, A. Furube, K. Hara, *Chem. Mater.*, 2008, 20, 3993.
- (5) L. Vayssieres, K. Keis, A. Hagfeldt, S. Lindquist, *Chem. Mater.*, 2001, 13, 4395-4398.
- (6) Z. R. Tian, J. A. Voigt, J. Liu, B. McKenzie, M. J. Mcdermott, *J. Am. Chem. Soc.*, 2002, 124, 12954-12955.
- (7) L. E. Greene, M. Law, J. Goldberger, F. Kim, J. C. Johnson, Y. Zhang, R. J. Saykally, P. Yang, *Angew. Chem. Int. Ed.*, 2003, 42, 3031-3034.